Collective, short-wavelength excitations in liquid gallium

F. J. Bermejo and R. Fernández-Perea
Instituto de Estructura de la Materia, CSIC, Serrano 123, E-28006 Madrid, Spain

M. Alvarez
Instituto Rocasolano, CSIC, Serrano 119, E/28006 Madrid, Spain

B. Roessli, H. E. Fischer, and J. Bossy
Institut Laue Langevin, B.P. 156x, F-38042 Grenoble Cedex 9, France
(Received 22 October 1996; revised manuscript received 20 December 1996)

Well-defined (i.e., not overdamped) collective excitations have been found in liquid Ga at 973 K (about 670 K above the melting point) by means of inelastic neutron scattering. The experimental results contrast with a previous investigation carried out at $T=326$ K (only 23 K above melting) where only heavily damped excitations were found, and partially agree with those of recently reported *ab initio* simulations for the high-temperature liquid. The interpretation of the experimental data is aided by results from a molecular dynamics simulation, which is carried out using an effective potential derived by inversion of the measured static structure factor. A comparison of experimental and simulation data reveals the mostly nonacoustic character of the excitations appearing at higher frequencies.
[S1063-651X(97)13209-3]

PACS number(s): 61.25.Em, 63.50.+x

I. INTRODUCTION

The collective behavior of semimetals (Sb, Bi, Te, Ga), as well as that of some group-IV elements (i.e., Si, Ge), shows a number of features that still resist a full quantitative understanding. Among the former group, the case of solid and liquid Ga (l-Ga) seems paramount. Being a trivalent element, gallium is one of the few metalliclike solids that does not crystallize into any simple structure. It shows instead an extremely rich polymorphism that includes a stable, low-pressure (atmospheric) phase, α-Ga, of orthorhombic *Cmca* structure with eight atoms per unit cell [1] (somewhat reminiscent of that shown by iodine), and two other phases which are stable at high pressure [2] (a body centered cubic phase with twelve atoms per unit cell known as Ga II, and a tetragonal phase called Ga III showing a structure very much like that of β-tin) [2]. Furthermore, a number of metastable phases known as β, γ, δ, and ϵ with melting points of 256.8, 237.6, 253.8, and 244.6 K (all well below that of 302.93 K for α-Ga) have been reported [3]. More specifically, β-Ga shows a C-centered monoclinic $C2/c$ crystal structure with two atoms in the primitive unit cell, whereas γ-Ga shows a *Cmcm* orthorhombic structure with 40 atoms per unit cell and δ-Ga has a $R\bar{3}m$ rhombohedral structure with 22 atoms in the unit cell [3].

Such an intricate phase diagram seems to imply the presence of complicated atomic forces, substantially distinct from those characteristic of simple, nearly-free-electron (NFE) metals. In fact, as revealed by photoemission experiments and reproduced in calculations [4,5], the electronic density of states of α-Ga shows a pseudogap at the Fermi level, often interpreted as indicative of a partial covalent character. Such partial covalency of α-Ga has been shown to give way to a far more metallic character as one goes through the sequence [5] α-G$a\rightarrow\beta$-Ga$\rightarrow$Ga II $\rightarrow$Ga III$\rightarrow$l-Ga (liquid-Ga), the latter showing an electronic density of states that approaches that of a NFE system [6,4,5], even if the presence within the liquid of very short-lived Ga_2 dimers, which are considered as remnants of those characteristic of α-Ga, has been postulated from *ab initio* simulations [6]. It is therefore the simultaneous presence of two kinds of bonding (i.e., metallic versus covalent) that makes the physics of condensed Ga, and particularly that of its noncrystalline phases, extremely interesting. As summarized in Ref. [7], the thermodynamic, electronic, and superconductive behavior of the metastable phases are substantially closer to those of l-Ga and amorphous (a-Ga) [8] than that of the stablest α-G form, and in particular those of β-Ga are thought to resemble in many respects those found in the disordered phases [9].

On the other hand, the liquid displays a number of remarkable features, such as a density increase of about 2.9% upon melting, a rather wide liquid range (2270 K), as well as a remarkably small change in the electronic transport properties upon melting. In fact, the electrical resistivity of α-Ga is extremely anisotropic, showing ratios along the three crystal axes of $\rho_e^c:\rho_e^a:\rho_e^b=1:0.32:0.14$, such that upon melting at $T_m=302.93$ K, the isotropic (liquid) value for this transport property corresponds to a decrease by 0.45 times the value along the c axis, and an increase by 1.46 and 3.12 times [10] the values along the crystal a and b axes, respectively.

Under appropriate conditions the liquid can be supercooled down to one-half of its normal T_m, and an amorphous phase can be formed by vapor deposition on a cold substrate [8], which crystallizes upon heating into the metastable β-Ga form [11]. The β phase shows a stability larger than that of the liquid (or the amorphous solid) and thus

constitutes an intermediate step in the process through which translational order sets in and therefore can be considered as a necessary step in the relaxation towards final equilibrium [12] encompassed in the stablest α-Ga.

The present paper thus aims to explore the extent to which some remnants of the dynamics of the crystal phases still persist in the high-temperature liquid. The collective dynamics of the α phase (stable) has been studied in detail using inelastic neutron scattering (INS) by Waeber and others [13], whereas the β phase was explored by Bosio *et al.* [9]. The interest of our exercise stems from the somewhat paradoxical circumstance that portrays β-Ga as a form closer to the disordered phases than α-Ga, with respect to most of the elastic, thermal, and transport properties [7], whereas the presence within the liquid of a measurable portion of Ga dimers [6] renders the liquid closer to some aspects of the stable crystal. We have therefore performed INS measurements on the liquid phase to compare its collective dynamics to that of the α and β phases.

A previous INS investigation [14] was carried out at temperatures close to melting (326 K), since, in analogy to a number of liquid metals explored so far [15], it was expected that these were the optimal conditions for observing well-defined collective density oscillations. However, the experiment only showed broad, overdamped features, in stark contrast to the $S(Q,\omega)$ dynamic structure factors calculated via a molecular dynamics (MD) simulation using the effective interaction potential derived from inversion of the experimental $S(Q)$ static structure factor [16]. Another, more recent simulation, this time *ab initio* [6], predicted the presence of well-defined excitations at temperatures well above melting (702 and 982 K) showing a dependence with wave vector reminiscent of a sound-mode excitation. As postulated in [14] and also commented upon in [6], the most likely reason for the discrepancy between the 326 K experimental and the two MD simulations may be the large bulk viscosity, which is known to be characteristic of some semimetals such as Bi [17] and which is expected to decrease markedly as the temperature is raised. In fact, from estimates of the shear and bulk coefficients of viscosity computed from derivatives of the effective potential and radial distribution functions [14], it was shown that the ratio η_B/η_s of bulk to shear viscosities decreased from 4.71 at $T=326$ K down to 1.16 at $T=956$ K. From tabulated values of the shear viscosity [18] one then gets estimates for η_B that go from about 9.4 mPa s just above melting to 0.7 mPa s at 956 K. Such a remarkable decrease will thus result in a drop of the damping term, which on hydrodynamic grounds can be written as

$$\Gamma_Q=\frac{Q^2}{2\rho}\left[\frac{4}{3}\eta_s+\eta_B+\lambda(\gamma-1)/C_p\right], \tag{1}$$

where ρ stands for the ionic number density, γ for the ratio of specific heats at constant volume and pressure (C_v,C_p), and λ is the thermal conductivity. The last term in the above expression shows a far milder variation with temperature than the viscosities since $\gamma=1.08$ at the melting point and approaches 1 at high temperatures. So, the increase in λ/C_p by about 2.5 times between melting and 1000 K will not counterbalance the strong drop in η_B, which in addition to that of the shear component will cause a reduction in the value of the longitudinal viscosity by a factor of approximately 7.3.

II. EXPERIMENTAL AND COMPUTER SIMULATION DETAILS

The neutron measurements were carried out using the IN8 and IN1 thermal and hot-neutron triple-axis spectrometers (TAS) of the Institut Laue Langevin, both operated in the final constant-wave-vector (k_f) mode. Initial measurements were performed using $k_f=6$ and 7 Å^{-1} on TAS IN8, but the final results were obtained with the IN1 instrument, which offers more intensity at high-energy transfers and also enabled us to employ a larger final wave vector k_f. This was required as spectra measured on IN8 showed a rather wide inelastic component extending up to several tens of meV at relatively small momentum transfers (e.g., about 25 meV at $Q\approx1$ Å^{-1}) compared with Q_p [i.e., the Q value corresponding to the maximum in $S(Q)$], and therefore a wider range of energy transfers was required for an adequate characterization of the excitations.

The spectrometer configuration [19] was chosen to optimize focusing conditions (resolution in energy transfers) commensurate with the dispersion curves shown in Fig. 6 of [6] and Cu (200) crystals were in all cases employed as monochromator and analyzer, respectively. The optimal experimental conditions were found after a number of tests employing different sets of collimations and final wave vectors. These were those with $k_f=7.1$ Å^{-1}, using the vertical focusing Cu (200) monochromator and analyzer, and a collimation of 20′ (in pile)–40′ (between monochromator and sample)–20′ (between sample and analyzer)–20′ (between analyzer and detector). The energy resolution at the elastic peak position was 5.5 meV [full width at half maximum (FWHM)] on TAS IN1, as measured with a vanadium sample. Such a value was only 0.3 meV away from that calculated analytically using the spectrometer configuration parameters [20].

The 70 g sample was held in a Nb flat plate cell of 36 mm width, 65.5 mm height, and 4 mm breadth (parallel to the beam) made of 0.5 mm Nb plate. The sample container was installed in a standard ILL furnace, the tail of which was surrounded by a 1 m diameter vacuum tank employed to reduce air scattering and thus allow a smaller detector angle for low-Q measurements. Particular attention was paid to the precise measurement of the empty cell in order to allow accurate subtraction of this contribution. The latter amounts to about 3% of the inelastic intensity at 20 meV and 1.5 Å^{-1}, which corresponds to the maximum contribution arising from phonons of polycrystalline Nb.

Finally, consideration of the relatively large wave-vector-transfer employed (7.1 Å^{-1}) and the range of frequencies explored (below 50 meV) ensures that no contamination due to higher-order effects (that is, for instance, when $2k_f=k_i$) is present in the measured response. This happens as a consequence of both neutron kinematics and the low flux at the higher end of the spectrum (above 400 meV or ≈13.9 Å^{-1}) on this spectrometer. Furthermore, the absence of features of spurious origin is also borne out by the different setups employed in the two different spectrometers. In

fact, it is expected that any artifactual contribution to the scattering will show a strong dependence with some relevant instrumental parameter (especially k_f). As we repeated scans on different spectrometers and incident wave vectors and observed the same inelastic scattering, this provides an additional test demonstrating the physical soundness of the measured inelastic scattering.

In order to process the experimental intensities and convert them into physically interpretable magnitudes, the values of the nuclear coherent $\sigma_{\rm coh}$ and incoherent $\sigma_{\rm inc}$ scattering cross sections for thermal neutrons are needed. In the case of Ga, information regarding $\sigma_{\rm inc}$ is only approximate (see Table II of Ref. [16]). From the set of published values for both $\sigma_{\rm coh}$ and $\sigma_{\rm inc}$ we have adopted those of Koester *et al.* [21], which seem to be the only set compatible with static structure data [16].

The data were converted into dynamic structure factors using the experimental value of $S(Q)$ for normalization purposes [16], after subtraction of the scattering from the sample cell and all other sources of background. The total absorption coefficient for the sample was found to be $\mu_T = 0.40\ {\rm cm}^{-1}$, which yields a transmission somewhat above 85%. Multiple scattering was estimated using the method of Blech and Averbach [22] for an incident energy of 104.4 meV ($=2.0717 k_f^2$). It was found to contribute to less than 6% of the total intensity and was therefore neglected. Such an estimate is consistent with that corresponding to our previous experiment [14] where a far thicker sample also having a larger density was employed. The scans were performed in the constant-Q mode covering a range of momentum transfers $0.7\ {\rm Å}^{-1} \leqslant Q \leqslant 4.0\ {\rm Å}^{-1}$ that comprises the first two peaks in the static structure factor. A total of 15 different wave vectors were in this way measured for $T = 973$ K. Measurements were set to a total of 40 000 monitor counts, which involved counting times of 5–7 min per data point, depending upon the required incident energy. The $I(Q, \omega = 0)$ elastic intensity was measured several times between runs in order to confirm the stability of the sample in the beam.

An initial set of six runs was carried at a temperature of $T = 700$ K, to provide a direct comparison with previous measurements using TAS IN8. The spectra measured at such a temperature were found to be in full agreement with those measured previously. A broad inelastic background far better defined than those reported for lower temperatures [14] was there seen. However, the analysis of such spectra yielded frequencies-to-damping ratios $\omega_Q / 2\Gamma_Q$ of 0.64, 0.54, and 0.53 for wave vectors of 0.8, 1.2, and 1.4 ${\rm Å}^{-1}$, respectively, which correspond to a strong damped regime (albeit not overdamped).

Finite-frequency excitations, that is, those with characteristic frequencies comparable to or smaller than their widths, were finally observed at the temperature $T = 973$ K.

A set of corrected spectra is shown in Fig. 1 where apart from a resolution-broadened quasielastic peak, a relatively strong inelastic contribution is clearly apparent. This inelastic intensity increases as Q approaches the first peak of $S(Q)$, which is centered about $Q_p \approx 2.5\ {\rm Å}^{-1}$. At momentum transfers below $0.7\ {\rm Å}^{-1}$ most of the inelastic signal is lost mainly because of the rather small value of $S(Q)$ below such a Q value, which causes the coherent response to be

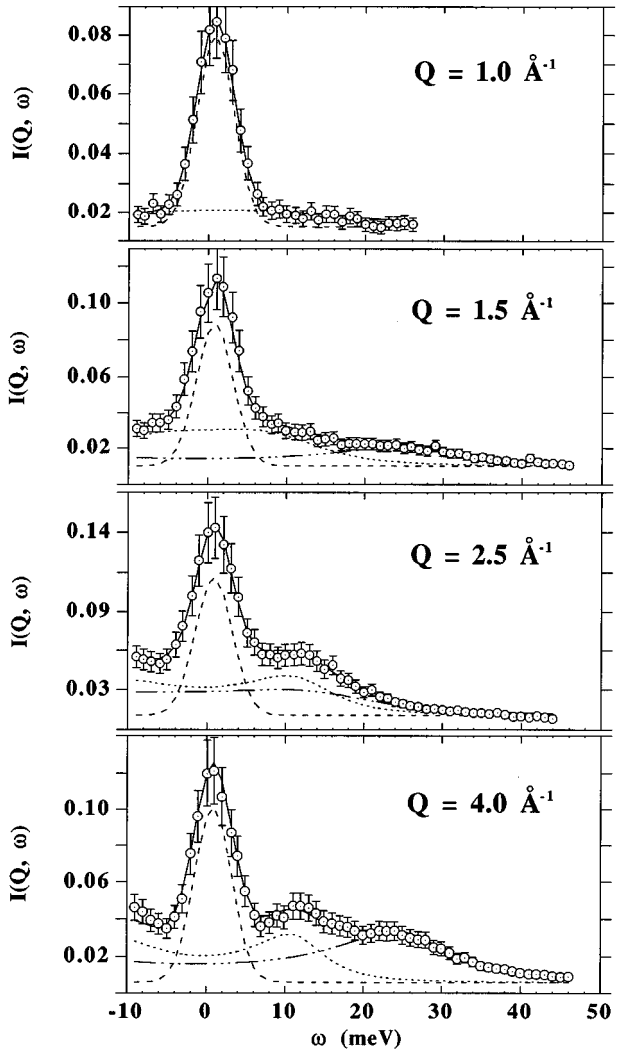

FIG. 1. A representative set of spectra measured using the IN1 spectrometer under conditions described in the text, for different values of the momentum transfer Q and $T = 973$ K. The experimental measurements are depicted by the circles with a dot, and the fitted model by a solid line. All but the data in the uppermost graph have been fitted with two DHO's. The inelastic components of the fits are given by dotted and/or dash-dotted lines depending on whether only one or two DHO functions were required to fit the spectra. The fitted quasielastic intensity is shown by a dashed line. Note that the calculated curves are referred to the background level as a baseline. The relative importance of the latter can easily be gauged by inspection of the wings of the quasielastic component.

swamped by a quasielastic contribution of incoherent origin [for Ga $\sigma_{\rm inc}/(\sigma_{\rm inc}+\sigma_{\rm coh}) = 0.0658$]. Moreover, for Q values below $0.6\ {\rm Å}^{-1}$ measurements would also be limited by the neutron kinematics.

To assess the reliability of the measured intensities, Fig. 2 shows the wave vector dependence of the (resolution-broadened) $I(Q, \omega = 0)$ peak as well as the frequency integral of the remaining intensity of inelastic origin. Although the quantities plotted in Fig. 2 cannot be directly interpreted in terms of physical magnitudes (a correction for the resolution effects and a separation between coherent and incoherent components would then be required), they serve to dem-

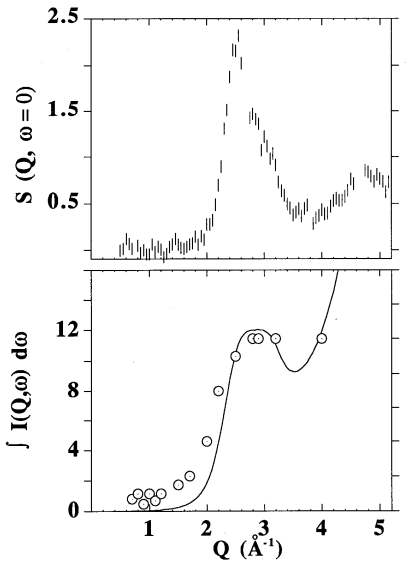

FIG. 2. The upper frame shows the elastic scan $S(Q,\omega=0)$ as measured on TAS IN8. The lower frame displays a comparison between the integrated inelastic intensities (symbols) and the quantity $Q^2S(Q)$ evaluated from the static structure factor given in [16].

onstrate that the measurements are free from spurious components. In fact, the quantity shown in the upper frame of Fig. 2 can be favorably compared with the static $S(Q)$ measured in Ref. [16] by diffraction means. On the other hand, the total inelastic intensity shown in Fig. 2 exhibits an oscillatory structure close to that of $Q^2S(Q)$, where the structure factor is taken from Ref. [16]. As will be discussed below, this can be taken as an indication of excitations of sound-mode origin, although contributions from other kinds of atomic motions are not ruled out.

The molecular dynamics simulation was performed with the DL-POLY program [23] for $T=973$ K using the effective pair potential for liquid gallium as derived from the experimental static structure factor $S(Q)$ through an iterative inversion procedure described in Ref. [16]. The simulation was performed with a system of 500 Ga atoms embedded in a cubic box with dimensions corresponding to a density equal to the experimental value at the required temperature. The simulated dynamic structure factors $S(Q,\omega)$ as well as the single-particle $S_s(Q,\omega)$ were calculated from Fourier cosine transforms of the intermediate scattering functions for total $I(Q,t)$ and ''self'' $I_s(Q,t)$ correlations, which are defined as the time autocorrelation functions of the Fourier components of the density $\hat{\rho}_{\mathbf{Q}}$ as follows:

$$I(\mathbf{Q},t)=\langle\hat{\rho}_{\mathbf{Q}}(t)\hat{\rho}_{-\mathbf{Q}}(0)\rangle, \tag{2}$$

$$\hat{\rho}_{\mathbf{Q}}=\int \exp(-i\mathbf{Q}\cdot\mathbf{r})\rho(\mathbf{r})d\mathbf{r}=\sum_{j=1}^{N}\exp(-i\mathbf{Q}\cdot\mathbf{r}_j), \tag{3}$$

$$I_s(\mathbf{Q},t)=\langle\hat{\rho}^s_{\mathbf{Q}}(t)\hat{\rho}^s_{-\mathbf{Q}}(0)\rangle, \tag{4}$$

$$\hat{\rho}^s_{\mathbf{Q}}=\exp(-i\mathbf{Q}\cdot\mathbf{r}_s), \tag{5}$$

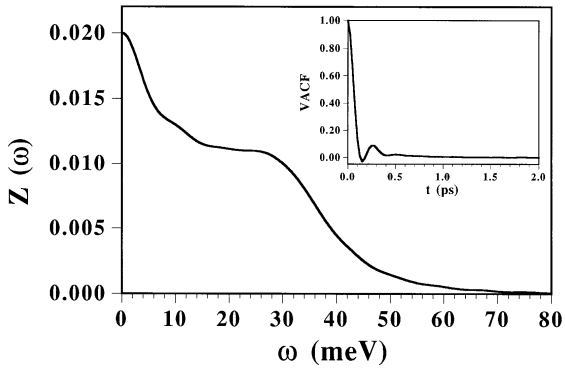

FIG. 3. The $Z(\omega)$ spectral frequency distribution of the MD simulations as calculated from the $\langle v(t)v(0)\rangle$ velocity autocorrelation function (shown as inset).

where N stands for the number of atoms, $\rho(r)$ the number density, and the superscript s denotes tagged-particle correlations. The $I(Q,t)$ was calculated from the atomic coordinates stored at regular intervals during the MD simulation following Eq. (2), i.e., performing both the time average and the orientation-average of $\mathbf{Q}$ at 25 fs intervals.

Not surprisingly, the MD simulation was able to reproduce the experimental static pair distribution $g(r)$ up to a high degree of accuracy, since its potential was derived from an experimentally measured $S(Q)$. To extend such a test to some dynamical properties we also calculated the self-diffusion coefficient from the time-dependent mean square displacements. The value obtained was 1.015×10^{-4} $\mathrm{cm}^2\,\mathrm{s}^{-1}$, which seems to be in rather good agreement with the experimental value of 1.3×10^{-4} $\mathrm{cm}^2\,\mathrm{s}^{-1}$, and smaller than estimations previously reported in the literature [24]. Such a relatively large self-diffusion coefficient is also reproduced in the $\omega\rightarrow 0$ intercept of the $Z(\omega)$ generalized frequency spectrum shown in Fig. 3 calculated from the $\langle v(t)v(0)\rangle$ atomic-velocity autocorrelation function (VACF). The calculated $S_s(Q,\omega)$ shows a line shape that can be adequately represented by a Lorentzian up to $Q\approx2$ Å^{-1}. Its linewidth follows a Fickian behavior $[\Gamma_t^{\mathrm{calc}}(Q)=D_t^{\mathrm{calc}}Q^2]$ up to relatively high wave vectors (~1 Å^{-1}) bending towards a constant value at higher Q's. In terms of a shape parameter such as $\Gamma_t^{\mathrm{calc}}(Q)S_s^{\mathrm{calc}}(Q,0)$, the simulated data seem to indicate a departure from classical (Fickian) diffusion taking place at fairly low wave vectors ≈1.2 Å^{-1}, a phenomenon common to some other metals explored so far (see Gläser in [15]).

A set of calculated spectra covering the most significant portions of the region of wave vectors of interest is shown in Fig. 4. Note that the curves on the right-hand side of the figure represent coherent scattering only. A detailed comparison between experiment and simulation is difficult because of the poorly determined value of σ_{inc} (the values listed in Table II of [16] show a mean of 0.39 b and a standard deviation of 0.38 b). Taking the $\sigma_{\mathrm{inc}}=0.47$ b from [21] the total spectrum containing coherent and incoherent contributions can be calculated, thus enabling a comparison between the single-particle and collective responses in the measured quantity. A glance at those spectra as well as at those shown in Fig. 1 seems to indicate that although the structure of experimental and simulated spectra below about 1.5 Å^{-1}

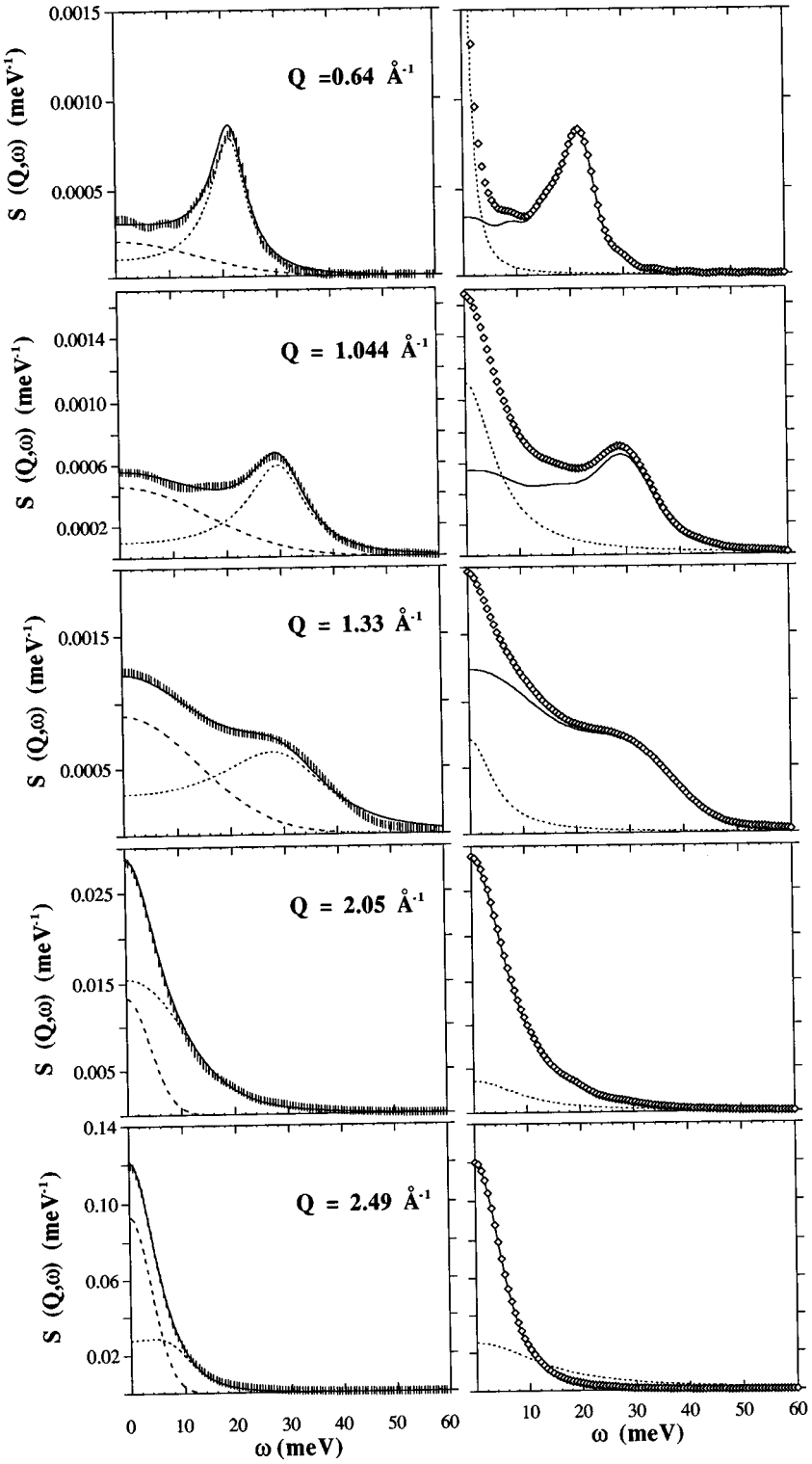

FIG. 4. The left-hand side shows a set of $S(Q,\omega)$ dynamic structure factors as calculated from the MD simulations corresponding to wave vectors well below, half-way up, and at the top of the $S(Q)$ static structure factor. The MD data are shown as vertical bars, the best-fit model as a solid line, the inelastic component given by one DHO function as a dotted line, and the quasielastic response as a dashed line. The right-hand side compares the coherent $S(Q,\omega)$ (solid line) and $S_s(Q,\omega)$ single-particle contributions to the total spectra (symbols). Scaling of the coherent and incoherent responses follow cross-section data of [21].

is not too dissimilar, the incoherent scattering contribution is clearly underestimated.

III. RESULTS

A. Experiment

The experimental spectra were analyzed in terms of a model that accounts for coherent and incoherent contributions to the total double differential cross section and is given by

$$I_{\mathrm{obs}}(Q,\omega)=A\left[\left.\frac{d^2\sigma}{d\omega d\Omega}\right|_{\mathrm{coh}}+\left.\frac{d^2\sigma}{d\omega d\Omega}\right|_{\mathrm{inc}}\right]\otimes R(Q,\omega)+B, \tag{6}$$

where A represents a global scaling constant and the symbol $\otimes$ stands for convolution with the $R(Q,\omega)$ resolution function of the spectrometer and B is a constant (frequency-independent) background. Both coherent and incoherent contributions are then expressed in terms of the relevant dynamic structure factors as

$$\left.\frac{d^2\sigma}{d\omega d\Omega}\right|_{\rm coh} = \sigma_{\rm coh} S_{\rm coh}(Q,\omega) = \sigma_{\rm coh}[S^0(Q,\omega) + S^1(Q,\omega)], \tag{7}$$

$$\left.\frac{d^2\sigma}{d\omega d\Omega}\right|_{\rm inc} = \sigma_{\rm inc} S_{\rm inc}(Q,\omega) = \sigma_{\rm inc}[S_I(Q,\omega) + S_M(Q,\omega)], \tag{8}$$

where $\sigma_{\rm coh,inc}$ stand for the coherent and incoherent neutron cross sections, respectively.

The coherent scattering has been approximated as resulting from two contributions, $S^0(Q,\omega)$ and $S^1(Q,\omega)$, which represent the zeroth- and finite-frequency contributions (single excitation). The former term corresponds to coherent quasielastic scattering, which is modeled as done before using the Kerr approximation [14], whereas the latter term follows a description of the liquid dynamics in terms of damped harmonic oscillators (DHO) [25]

$$S^1(Q,\omega) = H_Q n(\omega) \frac{4\omega\omega_Q^2\Gamma_Q^2}{(\omega^2-\omega_Q^2)^2 + 4\omega^2\Gamma_Q^2}, \tag{9}$$

with H_Q the strength of the single-phonon excitation, $n(\omega) = [1-\exp(-\hbar\omega\beta)]^{-1}$ the thermal occupation factor [$\beta = (k_B T)^{-1}$], and ω_Q the oscillator bare frequency having a linewidth specified by the damping coefficient Γ_Q. The physical frequency of such an oscillator is given by the quantity ω_Q, which in the present case has to be interpreted as an average frequency corresponding to the center of gravity of the manifold of excitations under consideration. The damping coefficient Γ_Q gives a measure of the apparent broadening in terms of homogeneous (originating from excitations of a single mode with a finite lifetime) and heterogeneous (originating from excitations of different frequencies) contributions, which cannot be resolved.

The incoherent scattering given in Eq. (8) is modeled using the simple hydrodynamic formula:

$$S_I(Q,\omega) = S_{\rm inc}^{\rm quel}(Q,\omega) = S_{\rm trans}(Q,\omega) = \frac{1}{\pi}\frac{\Gamma_t(Q)}{\omega^2+\Gamma_t^2(Q)},$$

$$\Gamma_t(Q) = \frac{D_t Q^2}{1 + D_t Q^2 \tau_0}, \tag{10}$$

where $S_{\rm trans}(Q,\omega)$ represents the contribution from the translational motion, approximated by a random-jump-diffusion model and contains as free parameters the self-diffusion coefficient D_t and the residence time τ_0. Because of the relatively low resolution in energy transfers achieved in the present experiment, no information could be derived from the analysis of the quasielastic width. Therefore, the value for D_t was set to the estimate given above, leaving only τ_0 adjustable in order to account for the observed quasielastic shape.

The term $S_M(Q,\omega)$ represents a multiexcitation contribution that, at high temperatures, becomes substantial at large wave vectors. It was approximated following the standard procedure using the $Z(\omega)$ derived from the simulation as a kernel [26]. Note that both the multiexcitation and incoherent contributions as well as those regarding single-particle dynamics are adding only one adjustable parameter (in addition to those characterizing the inelastic wings) to the model scattering laws. The ratio of coherent quasielastic to inelastic intensities is governed by the values of the oscillator strength H_Q of Eq. (9), for which no closed form (sum-rule) expression is available because of the highly damped nature of the motions, although it is expected to show oscillations that are in phase with those of the $S(Q)$ static structure factor.

As a starting point for the data analysis, the inelastic spectra were fitted using a single spectral component (DHO). This procedure was able to account for the observations up to a momentum transfer of about 2.9 Å^{-1}, beyond which the model gives only a semiquantitative description of the measured spectra. The results of the least-squares refinements [using Eq. (7)] are shown in Fig. 5, which compares the fitted ω_Q frequencies with some magnitudes calculated from the interaction potential [16], as well as a straight-line dispersion expected for a simple liquid model. Figure 5 also depicts the Q dependence of the excitation damping factors and intensities. The latter show a partial agreement with what one could expect for an excitation strength H_Q corresponding to a simple-liquid ''mode'' of sonic origin with a well-defined wave vector; that is, the intensities exhibit an oscillation in Q not far from that shown by the static structure factor. The agreement has to be taken as semiquantitative at best, since the maximum of such a peak in H_Q lies about 0.4 Å^{-1} above that shown by $S(Q)$. On the other hand, apart from the inadequacy of such a simple liquid model to describe high-Q spectra, the ω_Q frequencies derived from the fits lie well above those given by

$$\langle\omega_0^2\rangle = \frac{\langle\omega^2\rangle}{S(Q)} = \frac{Q^2}{m\beta S(Q)}, \tag{11}$$

which, for a simple monoatomic liquid, approach $v_T Q$, where v_T stands for the isothermal sound velocity. In fact, the fitted frequencies lie within $\langle\omega_0^2\rangle^{1/2}$ and

$$\langle\omega_l^2\rangle^{1/2} = \left[\frac{\langle\omega^4\rangle}{\langle\omega^2\rangle}\right]^{1/2}, \tag{12}$$

where $\langle\omega^n\rangle$ refers to the nth frequency moments of the dynamic structure factor, and can be calculated explicitly from the static pair correlation function and the effective potential, both derived from the measured $S(Q)$ as explained in some detail by Refs. [14] and [16]. In quite the same way as $\langle\omega_0^2\rangle^{1/2}$, the approach towards hydrodynamics of $\langle\omega_l^2\rangle^{1/2}$ can be interpreted as a high-frequency sound velocity given by

$$v_\infty(Q) = [\langle\omega_l^2\rangle/Q^2]^{1/2} = \left[\frac{1}{\rho}\left(\frac{4}{3}G_\infty(Q) + K_\infty(Q)\right)\right]^{1/2}, \tag{13}$$

where $G_\infty(Q)$ and $K_\infty(Q)$ stand for the generalized (i.e., wave vector dependent) shear and rigidity moduli, and thus $v_\infty(Q)$ would correspond to the speed of sound that would be observed if the viscous contribution were negligible since the acoustic dispersion $v_s(Q)$ is bounded by [27]

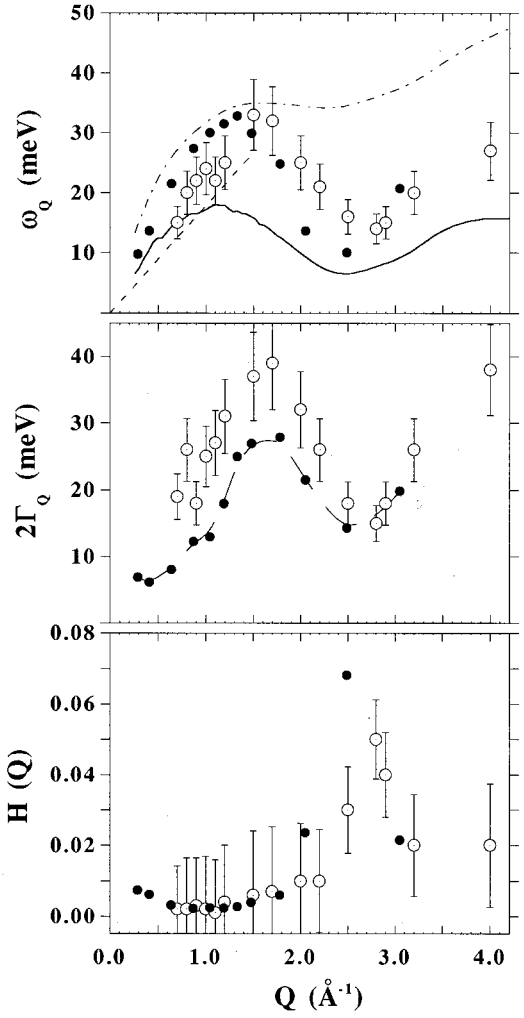

FIG. 5. The top frame depicts a comparison between experimental ω_Q frequencies (open symbols) using a single DHO to represent the inelastic side of the spectra with those calculated from the spectral moments of the structure factor (the solid line represents $\langle\omega_0^2\rangle^{1/2}$ and dashes refer to $\langle\omega_l^2\rangle^{1/2}$). The straight line depicts the dispersion of hydrodynamic sound (i.e., the simple liquid model). The filled symbols represent the oscillator frequencies derived from the analysis of computer-simulated spectra. The middle frame shows the wave vector dependence of the excitation linewidths and the lower frame gives their strengths. The symbol convention given above is retained.

$$v_s(Q)=\left[v_T^2(Q)+[v_\infty^2(Q)-v_T^2(Q)]\frac{\omega^2\tau_0^2(Q)}{1+\omega^2\tau_0^2(Q)}\right]^{1/2}. \tag{14}$$

Estimates for the $\tau_0(Q)$ relaxation time for the longitudinal viscosity calculated by means of the viscoelastic ansatz are given in Fig. 2(c) of [14] and show that, for the range of energy transfers explored here, such a magnitude is bounded within remarkably small values: 2×10^{-14} s$\leqslant\tau_0(Q)\leqslant5\times10^{-14}$ s, which makes the term containing $\omega^2\tau_0^2$ of the order of 10^{-2}, and therefore the speed of sound would have to be reasonably close to $v_T(Q)$.

B. Computer simulations

The results of the calculated dynamic structure factors $S(Q,\omega)$ in Fig. 4 show, up to wave vectors of ≈1.8 Å^{-1}, the presence of a clear inelastic peak having an apparent dispersion that is quantified in Fig. 5, where the analysis of the calculated spectra followed a procedure parallel to that employed for the experimental data.

As mentioned in previous paragraphs, the total intensity measured by experiment contains an additional contribution of incoherent origin, which arises mainly from zero-frequency (stochastic) motions. Because of the relatively high velocity of sound in liquid Ga, the zero-frequency component constitutes a large part of the total spectral power at low wave vectors [$S(0)=\rho k_B T\chi_T$, where ρ stands for the density and χ_T for the isothermal compressibility]. As a matter of fact, the small value of $S(Q)$ for low Q values [$S(Q)$ goes below 0.1 for wave vectors below 1.5 Å^{-1}] means that most of the low-Q spectrum will be dominated by the incoherent component, even if the ratio of total cross sections $\sigma_{\rm inc}/\sigma_{\rm coh}=0.0704$ still is somewhat modest.

From the calculated self-diffusion coefficient D_t, one can estimate a quasielastic width for translational diffusion having a wave-vector-dependent linewidth that in the Fickian regime (that is for Q values below 1 Å^{-1} or so) should behave as $\Delta\omega=D_tQ^2=0.67Q^2$ meV, and having an amplitude decreasing with Q, which, to first order, is expected to follow $(Q^2D_t)^{-1}=1.49Q^{-2}$ meV^{-1}.

Remarkably, even though the shapes of the experimental and simulated $S(Q,\omega)$ spectra are quite different, the ω_Q frequencies coming from both experiment and simulation are still rather close. Moreover, by looking at the well-defined peaks of Fig. 4, one can see that the fitted frequencies are close to those of the peak maxima, as expected.

As a matter of fact, in terms of quantities displayed in Fig. 5, the main differences between experiment and simulation concern the substantially larger damping terms of the former in the range of ≈0.8 Å$^{-1}\leqslant Q\leqslant1.6$ Å^{-1}. Note, however, that such magnitudes become comparable when approaching the hydrodynamic limit, something that may indicate that the longitudinal viscosity is not being grossly underestimated as was the case for the lower temperature study [14].

What seems worth stressing is the strong deviation from simple-liquid behavior exhibited by the simulation data since a ''dispersion curve'' not far from the one followed by $\langle\omega_0^2\rangle^{1/2}$ was expected. This would come as a consequence of the fact that both the simulated spectra and $\langle\omega_0^2\rangle^{1/2}$ arise resulting from the same two-body, empirical potential, and that by construction such a potential accounts, to high accuracy, for the hydrodynamic sound velocity [since it reproduces the isothermal compressibility as given by $\lim_{Q\to0}S(Q)$].

An indication of the existence, in the simulated spectra, of a complicated interplay between atomic movements that goes well beyond those exhibited by simpler metals is given by the frequency distribution $Z(\omega)$ depicted in Fig. 3. There an unusual feature in the form of a wide plateau between frequencies of about ≈20 and ≈30 meV is seen in the central frequency region. Such a characteristic contrasts with others measured or calculated for simpler liquid metals (see Ref. [28] for liquid Cs), where a well-defined (albeit broad)

maximum is seen at some finite frequency. On the other hand, the presence of a small shoulder at about 10 meV is also to be noticed. In terms of the $\langle v(t)v(0)\rangle$ shown in the inset of Fig. 3, the most remarkable feature concerns the rather fast decay of the atomic velocity correlations (about 0.1 ps the VACF enters the backscattering region where the direction of motions are reversed) as well as the rather quick loss of atomic correlations at times as short as 1 ps.

To better understand the microscopic origin of the excitations being sampled in the MD simulation, we also calculated the structure factors as $S(Q,\omega=\text{const})$ for selected values of the energy transfer. The interest in such an exercise lies in the fact that even for a liquid, which at such high frequencies can be expected to behave as an elastic solid, the constant-energy structure factors can be interpreted in terms of inelastic structure factors, paralleling that given in our previous report for the liquid just above melting [14]. As a consequence, the information contained in $S(Q,\omega=\text{const})$ can provide some details about the *geometry* of the atomic vibrations through the transform [29],

$$D^{\omega}(r)=\frac{2}{\pi}\int_0^{\infty} dQQ[S(Q,\omega=\text{const})/A-1]\sin(Qr), \tag{15}$$

with $A=\hbar Q^2/2M\exp(-\langle u^2\rangle Q^2/3)$. Here, M stands for the atomic mass and $\langle u^2\rangle$ for the atomic root-mean-square displacement of atoms involved in collective motions. The meaning of $D^{\omega=0}(r)$ is obvious: it corresponds to the static spatial correlation function of atoms $D^s(r)=4\pi\rho[g(r)-1]$ obtained by Fourier inversion of $[S(Q)-1]$. The peak positions in $D^s(r)$ correspond to the (thermal) average distance between atoms in the static structure as measurable in diffraction experiments [16]. In the case of in-phase displacements, such as those involved in sound-mode propagation, $D^{\omega}(r)$ will resemble $D^s(r)$ because the long-wavelength in-phase motion of atoms results in a uniform translation of the system, thereby yielding interatomic distances similar to the static configuration. At finite frequencies, however, relative displacements and out-of-phase motions of certain atoms will result in the disappearance of some of the peaks of the static structure and the emergence of new structure at other positions.

A set of $S(Q,\omega=\text{const})$ curves corresponding to characteristic zones of the ''dispersion curves'' shown in Fig. 5 is given in Fig. 6, and the corresponding $D^{\omega}(r)$ transforms are depicted in Fig. 7. A glance at such curves reveals that well-defined oscillations in phase with the static $S(Q)$ [or with its $S(Q,\omega=0)$ counterpart] persist up to relatively high frequencies (about 15 meV), and correspond to wave vectors of roughly $Q_p/4$ in the ''dispersion curve.'' At higher frequencies, such as those corresponding to the maximum in the ''dispersion curve'' (that is about 30 meV and $Q_p/2$), both the $S(Q,\omega=\text{const})$ and $D^{\omega}(r)$ functions show that the phase coherence with $S(Q)$ is progressively lost. As a consequence, most of the inelastic intensity arising from excitations about $Q_p/2$, should be regarded as nonacoustic (or ''optical'') in much the same way as those characteristic of Coulomb systems [31], whose existence was clearly revealed in inelastic neutron scattering experiments performed some time ago. On the other hand, the $D^{\omega}(r)$ real-space correlates

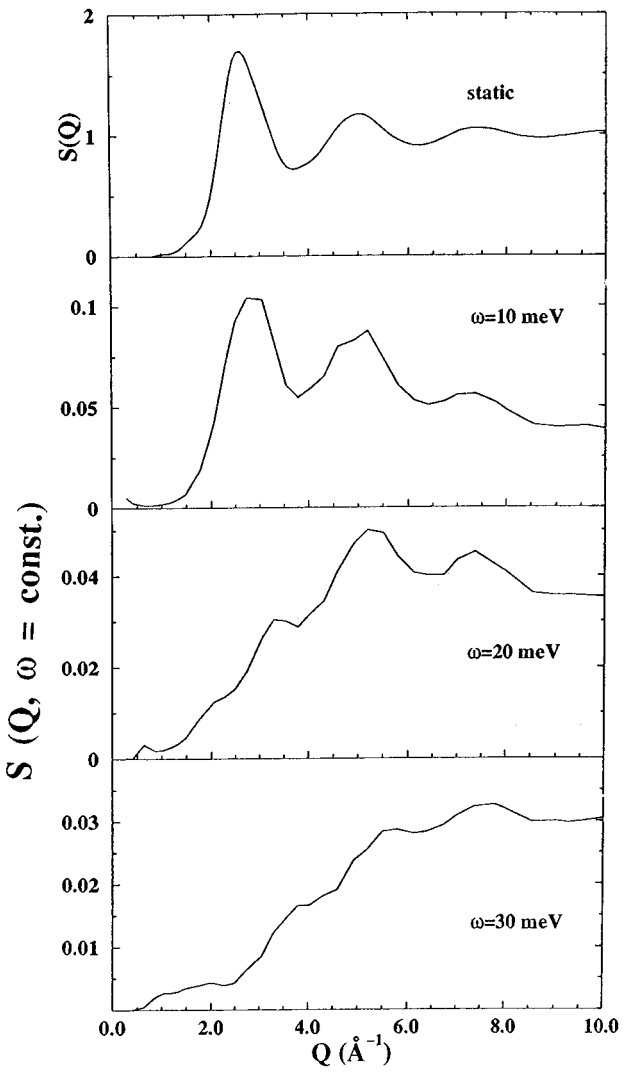

FIG. 6. The upper frame shows the static structure factor $S(Q)$ calculated from the instantaneous atomic positions. The bottom three curves show the functions calculated from the MD trajectories for nonzero energy transfers.

of $S(Q,\omega=\text{const})$ shown in Fig. 7 reveal a progression in the shape of the main peak of the static $D^s(r)$ at about 2.5 Å, which goes from a *mostly* in-phase behavior at 10 meV to a mostly out-of-phase peak at 30 meV, which involves atoms separated by ≈ 3 Å, while that at 20 meV is of a mixed character.

IV. DISCUSSION

The failure of the simple-liquid approach [i.e., that which predicts that only one kind of collective excitation persists in the liquid with frequencies given by Eq. (9)] to describe the high-frequency dynamics of this liquid material can also be seen from preliminary neutron time-of-flight (TOF) data reported years ago [32]. In fact, data for liquid Ga at $T=1253$ K [32] revealed the presence of a shoulder at wave vectors 3 Å$^{-1}\leqslant Q\leqslant 4$ Å^{-1} showing an apparent linear frequency dependence going from 18 meV up to approximately 23 meV within this Q range. Such data, which correspond to

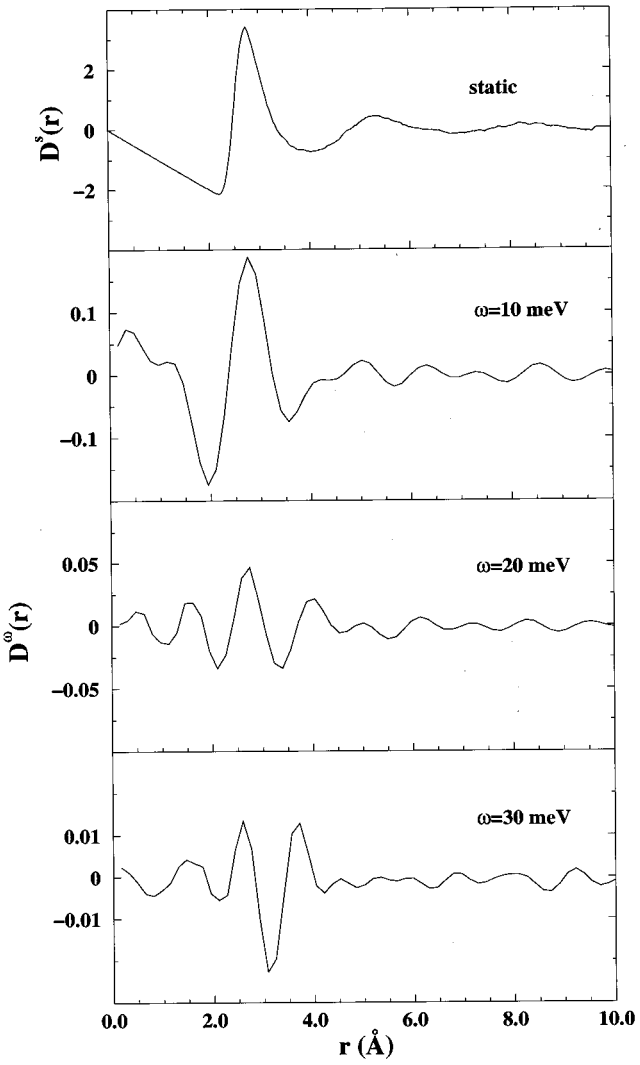

FIG. 7. The upper frame shows the static $D^s(r)$ function calculated from the instantaneous atomic positions in the MD simulation, being the Fourier transform of the results of the previous figure. The bottom three curves show the $D^{\omega}(r)$ functions for nonzero values of the energy transfer.

maxima in the experimental $\omega^2 S(Q,\omega)$, also lie well above the curve corresponding to $\langle\omega_0^2\rangle^{1/2}$, and thus provide an additional indication of the inadequacy of the simple-liquid picture to describe the dynamics of this liquid.

The reasons for such a discrepancy can be made clear by inspection of experimental data from a number of different sources. First, the inelastic intensity measured at constant energy transfer for liquid Ga at 330 K presented in Fig. 5 of [14] shows the presence of a well-defined feature for frequencies above 13 meV, which in no way can be considered as an acoustic mode since it shows a peak at about 4 Å^{-1} where the structure factor shows a minimum. Such frequencies also correspond to a well-defined but broad inelastic feature seen in TOF experiments [33]. A qualitative analysis of these $I(Q,\omega=\text{const})$ curves can be carried out on the basis of what is expected for a structure factor corresponding to a vibration of nonacoustic origin taking place at a given frequency ω, that is,

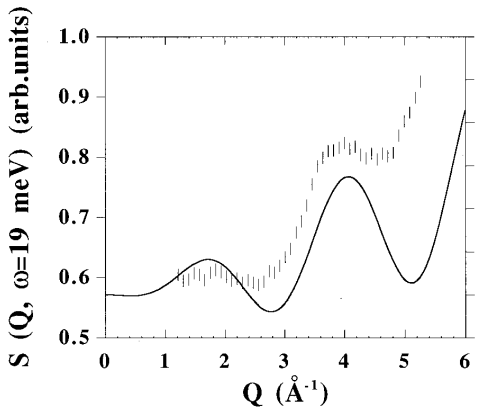

FIG. 8. A comparison between spectra for a constant energy transfer of 19 meV as measured during a previous experiment [14] (vertical bars), and as calculated using Eq. (16) (solid line). Note that the scaling between the two curves is arbitrary.

$$I^{\omega}_{\text{inel}}(Q)=\sum_{i,j}\frac{1}{3}(\mathbf{e}_i\cdot\mathbf{e}_j)[j_0(QR_{ij})+j_2(QR_{ij})]-\left(\frac{1}{R_{ij}}\right)^2(\mathbf{R}_{ij}\cdot\mathbf{e}_i)(\mathbf{R}_{ij}\cdot\mathbf{e}_j)j_2(QR_{ij}),\qquad(16)$$

where the sum runs over the (static) positions of all pairs of atoms, $R_{ij}=|\mathbf{R}_i-\mathbf{R}_j|$ is the relative distance between them, $\mathbf{e}_i$ is the displacement amplitude of atom i, and $j_{0,2}(x)$ are spherical Bessel functions. From the structure of Eq. (16) it is clear that at low Q values the first term containing a sum of $j_0(QR)+j_2(QR)=3j_1(QR)/QR$ dominates, and that a periodic modulation of the intensity of such a band can be expected following $j_1(QR)/QRj_2(QR)$, a ratio that will describe approximately the Q dependence of $I^{\omega}_{\text{inel}}(Q)$. Moreover, Eq. (16) also shows that for relatively large Q values (above 2.5 Å^{-1} or so), the second term containing the $(\mathbf{R}_{ij}\cdot\mathbf{e}_i)$ factor will be the dominant one and therefore one expects to find some revival of the inelastic intensities arising from excitations that depend upon the relative phases of such dot products and $j_2(QR)$, as experiments have shown. In fact, a calculation on qualitative grounds using Eq. (16) employing as parameters the distance $R_{ij}=2.72$ Å [which corresponds to that where $g(r)$ shows its first maximum [16]], and a vector displacement of about 0.001 Å (corresponding to motions that are purely out of phase), gives an inelastic structure factor that reproduces the main features observed in the previous experiment, as Fig. 8 vividly exemplifies.

Having established the mostly nonacoustic nature of excitations appearing above about 15–20 meV, a description of the experimental intensities better than that provided by a unique DHO function was sought. Because two different frequency bands of quasielastic to $\sim$16 meV and 16 meV to 50 meV clearly appear in the large-Q $S(Q=\text{const},\omega)$ spectra, as Fig. 1(b) clearly shows, an attempt to fit these two spectral regions using individual DHO functions to cover both ranges was pursued. As expected, decomposition of the whole inelastic response into two identifiable bands made sense only for relatively large Q values, that is for momentum transfers above $\approx$1.1 Å^{-1}. The results of such an analysis are shown

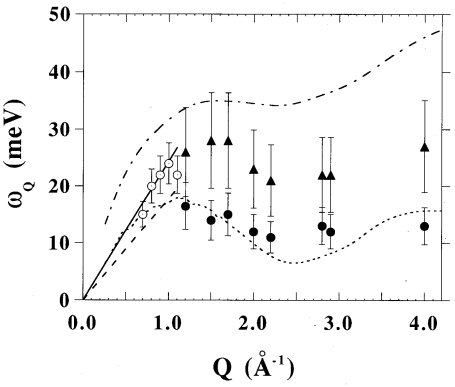

FIG. 9. The ω_Q frequencies derived from fits using two different descriptions of the inelastic spectra. The solid symbols represent the frequencies derived after decomposition of the inelastic intensity $S(Q,\omega)$ into two DHO functions. Circles with a dot represent the results for decomposition into a single DHO (see text). The dotted and dash-dotted lines represent the reduced second and fourth frequency moments as calculated from the empirical potential. The dashed straight line depicts the hydrodynamic sound dispersion and the solid line corresponds to an extrapolation to large wave vectors of the linear dispersion measured by light scattering [34].

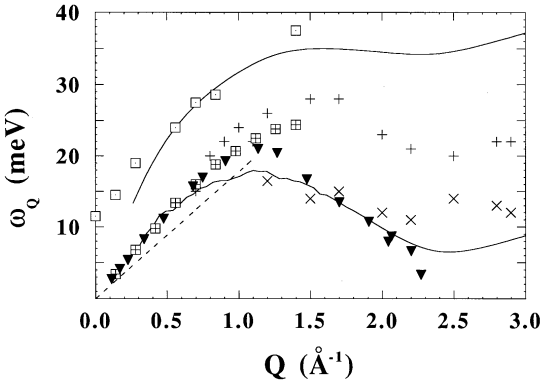

FIG. 10. A schematic comparison between the curves showing the phonon dispersion along $[\xi 00]$ in α-Ga [13] (squares with a dot stand for the $T_1^{(3)}$ optical branch, the squares with a cross represent the $T_1^{(1)}$ LA phonon) and that in β-Ga [9] (filled inverted triangles depict the LA_x branch over the Brillouin zone), along with data for the liquid. The thin solid lines represent $\langle\omega_0^2\rangle^{1/2}$ and $\langle\omega_l^2\rangle^{1/2}$, crosses refer to the ω_Q fitted frequencies, and the dashed straight line gives the hydrodynamic sound dispersion.

in Fig. 9. There, the wave vector dependence of the two frequencies employed for the description of the two damped oscillators is shown along with those employed to follow the ''dispersion curve'' at low wave vectors, where only one spectral component could be sensibly fitted to the data. A glance at Fig. 9 now reveals the presence of two ''dispersion curves,'' the lower frequency curve lying close to $\langle\omega_0^2\rangle^{1/2}$, and showing rather moderate dispersion. The shape and characteristic frequencies of such a ''dispersion curve'' are also in agreement with the one reported by Holender *et al.* [6], where the hydrodynamic sound is approached *from below*. The absence in the *ab initio* simulation of a higher-frequency component may well be due to the severe system-size and sampling-time limitations. As we will discuss below, the fact that the characteristic frequencies of this low-energy branch are close to some of the longitudinal acoustic modes of the α and β crystal phases gives strong support to the identification of such a ''dispersion curve'' with the one arising from the continuation of an acoustic mode down to this microscopic scale (i.e., high Q).

A point worth considering in some detail concerns results reported two decades ago on the propagation of hypersonic waves in liquid Ga (and Hg) as studied by means of Brillouin scattering of light [34]. There it was found that the apparent phase velocity of the hydrodynamic excitations was about 38% above that determined by ultrasound. In the case of liquid Ga, which was measured at $T=378$ K, well above T_m, the measured Brillouin frequencies seemed to follow a hydrodynamic dispersion $\omega_Q=cQ$ with $c=3700$ m s^{-1}. The authors of Ref. [34] tentatively attributed such an anomalously high velocity to some complicated dynamics taking place close to the liquid surface. However, plotting such linear dispersion together with the present data, as also done in Fig. 9, surprisingly reveals that data below about 1 Å^{-1} or so seem to follow such a law. Although a definite explanation of the origin of such high-frequency linear dispersion cannot be given, both the light-scattering and the present data point to some common mechanism that couples effectively the electromagnetic and neutron fields to these high-frequency excitations, which on the other hand become uncoupled to the compressional fields generated in mechanical spectroscopy experiments such as those reported in Ref. [30].

A correlation in $Z(\omega)$ of the two aforementioned frequency bands may also be seen from Fig. 3. In fact, most of the frequencies of the lower branch shown in Fig. 9 seem to be those that give rise to the weak shoulder centered about 10 meV in the frequency spectrum.

The presence of two distinct inelastic bands in the spectrum of this liquid at high Q is somewhat reminiscent of some observations on molten salts [31], which showed a clearly non-acoustic component having an apparent dependence with wave vector not too different from that shown in Fig. 9. An unambiguous assignment of the origin of the higher-frequency band seems beyond reach, taking into account the complicated patterns experimentally observed for the phonon dispersion relations in both α [13] and β [9] crystal phases. However, a comparison between single-crystal data and the observations for the liquid can be pursued on purely qualitative grounds. To this end, Fig. 10 shows a comparison between the reduced frequency moments as calculated from the effective potential [14,16], the fitted ω_Q frequencies and some representative phonon branches of α- and β-Ga [9,13] corresponding to the $[\xi 00]$ propagation direction in both crystals. The remarkable coincidence of the LA_x phonon in the metastable β-Ga with the curve for the $\langle\omega_0^2\rangle^{1/2}$ second reduced frequency moment of the liquid came as a surprise, and the same qualification applies to the $T_1^{(3)}$ optical branch of α-Ga with respect to $\langle\omega_l^2\rangle^{1/2}$. Also worth mentioning is the close proximity of the dispersions of both LA_x and $T_1^{(3)}$ phonons, if one considers the rather different mechanical, thermal, and even density differences between the two crystalline solids.

As a result of the comparison mentioned in the previous

paragraph, some parallelism between the microscopic dynamics of liquid and crystalline Ga may be established, at least on qualitative grounds. If, as argued by some [3], liquid Ga were to be structural and dynamically closer to β-Ga than to α-Ga, then excitations above 23 meV or so (e.g., the frequency corresponding to the highest energy phonon, a TO_y branch in β-Ga) should not be present in the experimental spectra. However, the observed long inelastic tails, which stretch up to frequencies that are about twice that boundary, seem to provide an indirect confirmation of the presence of instantaneous liquid configurations that give rise to atomic motions reminiscent of those observed in the α phase.

The present results also seem to be of relevance for the understanding of the microscopic properties of liquid Hg, which shows a number of macroscopic properties such as specific heat, atomic volume, and shear viscosity not too far from those shown by liquid Ga [35]. Even more, the same anomalous behavior *vis-a-vis* the sound velocity observed for liquid Ga has also been reported for liquid Hg [34], and a recent neutron scattering experiment did not directly reveal the presence of well-defined excitations [36].

V. CONCLUSIONS

The present work provides an example of how the microscopic dynamics of a relatively complicated monoatomic liquid can be better understood by recourse to the crystal dynamics rather than to theoretical constructs applicable only to simple liquids. In fact, the intercomparison of data shown in Fig. 10 shows that the collective dynamics of this liquid cannot be understood solely in terms of sound modes, as in the case of simple molten alkali metals. Additional, high-frequency excitations of nonacoustic origin contribute with substantial amplitudes to the dynamic structure factor, and this makes inadequate the interpretation of v_∞ given by Eq. (13) as a high-frequency sound velocity. The present results thus constitute a warning against oversimplified interpretations of frequencies well above those corresponding to hydrodynamic sound that result from the analysis of experimental or simulation data in terms of phenomena predicted to appear under rather special conditions (e.g., ''fast-sound'' in liquids) in simpler systems (e.g., binary mixtures of hard spheres). In addition, we have demonstrated the utility of MD simulations that employ an effective potential derived from the experimental $S(Q)$.

ACKNOWLEDGMENTS

This work has been supported in part by Grant No. PB95-0072-c03-01 (Spain). M.A. wishes to acknowledge support by the Spanish Dirección General de Investigación Científica y Técnica (DGICYT) under Grant No. PB94-0112. Dr. E. Lomba is kindly acknowledged for his help on technical details concerning computer simulation as well as Professor M.C. Bellisent-Funel for providing us with numerical data for the effective potentials. We would also like to thank P. Palleau for assistance with the IN1 experiment, J. Loppé for his help in obtaining the Nb sample container, and the furnace group of the ILL (P. Andant and P. Martin).

[1] C. S. Barret and F. J. Spooner, Nature (London) **207**, 1382 (1965).

[2] L. Bosio, J. Chem. Phys. **68**, 1221 (1978).

[3] L. Bosio, A Defrain, H. Curien, and A. Rimsky, Acta Crystallogr. Sect. B **25**, 995 (1969); L. Bosio, H. Curien, M. Dupont, and A. Rimsky, *ibid.* **28**, 1974 (1972); **29**, 367 (1973). The structure of ϵ-Ga does not seem to be known in detail at present.

[4] F. Greuter and P. Oehlhafen, Z. Phys. B **34**, 123 (1979); G. Indlekofer, P. Oelhafen, R. Lapka, and H. J. Guntherodt, Z. Phys. Chem. N. F. **157**, 465 (1988). Calculations regarding these quantities are also reported by J. Hafner and W. Jank, Phys. Rev. B **42**, 11 530 (1990). Recent x-ray photoemission and bremsstrahlung isochromat spectroscopic results are given by S. R. Barman and D. D. Sarma, Phys. Rev. B **51**, 4007 (1995).

[5] M. Bernasconi, G. L. Chiarotti, and E. Tosatti, Phys. Rev. B **52**, 9988 (1995).

[6] J. M. Holender, M. J. Gillan, M. C. Payne, and A. D. Simpson, Phys. Rev. B **52**, 967 (1995). See also X. G. Gong, G. L. Chiarotti, M. Parinello, and E. Tosatti, Europhys. Lett. **21**, 469 (1993).

[7] A. Defrain, J. Chim. Phys. Phys.-Chim. Biol. **74**, 851 (1977); R. Cortés, Ph.D. thesis, University Paris VI, 1974 (unpublished).

[8] O. Hyunderi and R. Ryberg, J. Phys. F **4**, 2096 (1974). Some results of a MD simulation on rapidly quenched Ga are given in S.-F. Tsay, Phys. Rev. B **48**, 5945 (1993).

[9] L. Bosio, R. Cortés, J. R. D. Copley, W. D. Teuchert, and J. Lefebvre, J. Phys. F **11**, 2261 (1981).

[10] F. J. Bermejo, L. Fernandez-Barquin, J. Garcia-Soldevilla, D. Gómez-Plaza, and J. C. Gómez-Sal, Phys. Rev. E **50**, 1341 (1994).

[11] J. Berty, M. J. David, L. Lafourcade, and A. Defrain, Scr. Metall. **10**, 645 (1976); A. Bererhi, L. Bosio, and R. Cortés, J. Non-Cryst. Solids **30**, 253 (1979).

[12] For a discussion of these topics see I. Gutzow and J. Schmelzer, *The Vitreous State: Thermodynamics, Structure, Rheology and Crystallization* (Springer-Verlag, Berlin, 1995), p. 374.

[13] W. B. Waeber, J. Phys. C **2**, 903 (1969); W. Reichart, R. M. Nicklow, G. Colling, and H. G. Smith, Bull. Am. Phys. Soc. **14**, 378 (1969).

[14] F. J. Bermejo, M. García-Hernández, J. L. Martinez, and B. Hennion, Phys. Rev. E **49**, 3133 (1994).

[15] See, for instance, O. Söderstrom, U. Dahlborg, J. R. D. Copley, J. B. Suck, and B. Dorner, J. Phys. F **10**, L151 (1980); J. R. D. Copley and J. Rowe, Phys. Rev. A **9**, 1656 (1974); T. Bodensteiner, Ch. Morkel, W. Gläser, and B. Dorner, *ibid.* **45**, 5709 (1992); W. Gläser, in *Amorphous and Liquid Metals*, edited by E. Lüscher (Nijhoff, Dordrecht, 1985), p. 258.

[16] M. C. Bellisent-Funel, P. Chieux, D. Levesque, and J. J.

Weiss, Phys. Rev. A **39**, 6310 (1989).
[17] J. Jarzynski, Proc. Phys. Soc. London **81**, 745 (1963). See also W. Gudowski, K. E. Larsson, and M. Dzugutov, in *Static and Dynamic Properties of Liquids*, edited by M. Davidovic and A. K. Soper (Springer-Verlag, Berlin, 1989), p. 37.
[18] *Transportphänomene I, Viskosität von Flüssigkeiten*, Landolt-Börnstein, Vol. II, Part 5a (Springer-Verlag, Berlin, 1969), p. 126. Also see [35].
[19] For a brief description of the principles of operation of triple-axis spectrometry, see, for instance, C. Stassis, in *Methods in Experimental Physics*, edited by K. Sköld and D.L. Price (Academic, New York, 1986), Vol. 23A, p. 393.
[20] Program RESTRAX. Institut Laue Langevin software package (unpublished). The calculations are based in the formalism described by M. J. Cooper and R. Nathans, Acta Crystallogr. **23**, 357 (1967).
[21] L. Koester, K. Knopf, W. Waschkowski, and A. Klüver, Z. Phys. A **318**, 347 (1984).
[22] I. A. Blech and B. L. Averbach, Phys. Rev. **117**, 1113 (1964).
[23] DL-POLY is a package of molecular simulation routines written by W. Smith and T.R. Forester, Copyright the Engineering and Physical Sciences Research Council acting through its Daresbury and Rutherford Appleton Laboratory at Daresbury Laboratory 1994.
[24] J. Bosse, D. Quitman, and C. Wetzel, J. Phys. (Paris), Colloq. **41**, C8-378 (1980).
[25] Some other functional forms for a damped harmonic oscillator such as the one described in H. R. Glyde, *Excitations in Solid and Liquid Helium* (Clarendon Press, Oxford, 1994), pp. 184–185 are of use in the case when the inelastic intensity arises from single-mode excitations. In our case, where the measured intensity has to be ascribed to excitations of rather different characters, we made use of this simpler formula.
[26] S. W. Lovesey, *Theory of Neutron Scattering from Condensed Matter* (Oxford Science Publications, Oxford, 1986), p. 186.
[27] J. P. Boon and S. Yip, *Molecular Hydrodynamics* (Academic Press, New York, 1980), p. 303.
[28] R. Vallauri and F. J. Bermejo, Phys. Rev. E **51**, 2654 (1995).
[29] The procedure has been developed by J. M. Carpenter and C. A. Pelizzari, Phys. Rev. B **12**, 2397 (1975) and applied several times to the analysis of neutron scattering data from amorphous materials. See, for instance, A. C. Hannon, M. Arai, and R. G. Delaplane, Nucl. Instrum. Methods Phys. Res. A **354**, 96 (1995).
[30] M. Inui, S. Takeda, and T. Uechi, J. Phys. Soc. Jpn. **61**, 3203 (1992).
[31] R. L. McGreevy, E. W. J. Mitchell, and F. M. A. Margaca, J. Phys. C **17**, 775 (1984).
[32] W. Gläser, S. Hagen, U. Löffler, J.B. Suck, and W. Schommers, in *Proceedings of the International Conference on Liquid Metals* (Taylor and Francis, London 1973), p. 111.
[33] M. I. Barker, M. W. Johnson, N. H. March and D. I. Page, in *Proceedings of the International Conference on Liquid Metals* (Ref. [33]), p. 99. See also, W. Luzny, S. Niziol, J. Mayer, and I. Natkaniec, Phys. Status Solidi A **116**, K25 (1989).
[34] J. G. Dil and E. M. Brody, Phys. Rev. B **14**, 5218 (1976).
[35] T. Iida and R. I. L. Guthrie, *The Physical Properties of Liquid Metals* (Oxford Science Publications, Oxford 1993), p. 185.
[36] Ubaldo Bafile and Yaspal S. Badyal, ISIS Facility Report No. RAL-TR-96-050, 1996, p. A78 (unpublished).